

Closed-Loop Benchmarking of Stereo Visual-Inertial SLAM Systems: Understanding the Impact of Drift and Latency on Tracking Accuracy

Yipu Zhao¹, Justin S. Smith¹, Sambhu H. Karumanchi¹, and Patricio A. Vela¹

Abstract—Visual-inertial SLAM is essential for robot navigation in GPS-denied environments, e.g. indoor, underground. Conventionally, the performance of visual-inertial SLAM is evaluated with open-loop analysis, with a focus on the drift level of SLAM systems. In this paper, we raise the question on the importance of visual estimation latency in closed-loop navigation tasks, such as accurate trajectory tracking. To understand the impact of both drift and latency on visual-inertial SLAM systems, a closed-loop benchmarking simulation is conducted, where a robot is commanded to follow a desired trajectory using the feedback from visual-inertial estimation. By extensively evaluating the trajectory tracking performance of representative state-of-the-art visual-inertial SLAM systems, we reveal the importance of latency reduction in visual estimation module of these systems. The findings suggest directions of future improvements for visual-inertial SLAM.

I. INTRODUCTION

Vision-based state estimation techniques, such as Visual Odometry (VO) and Visual Simultaneous Localization and Mapping (VSLAM), are essential for robots to autonomously navigate through unmapped scenes. VO often forgets the sensed world structure, while VSLAM retains a long-term map of the traversed world. In the absence of absolute position signals such as from GPS, VO/VSLAM complements traditional wheel/inertial-based odometry.

Compared with VO/VSLAM that relies on vision sensor only, visual-inertial SLAM (VI-SLAM) uses the two complementary data streams to achieve better accuracy and robustness, and higher frequency, of state estimation. The visual sensor provides accurate, yet sparse and delayed measurements of absolute landmarks in the environment. Estimation drift is mitigated by observing and matching landmarks with a long but potentially intermittent measurement history. The inertial sensor provides high-rate, almost-instantaneous, yet drifting measurements of robot motion. Inertial measurements compensate for short duration visual feature loss (e.g. in texture poor settings). The pose estimates of a VI-SLAM system can be sent to a controller as a high-quality feedback signal in support of trajectory tracking as the mobile robot navigates through an environment.

While the ultimate use case of VI-SLAM in robotics is closed-loop navigation, traditional benchmarking of VI-SLAM employs open-loop analysis, i.e., the SLAM output doesn't affect actual robot actuation and future sensory input. Though reflecting the estimation drift level of VI-SLAM,

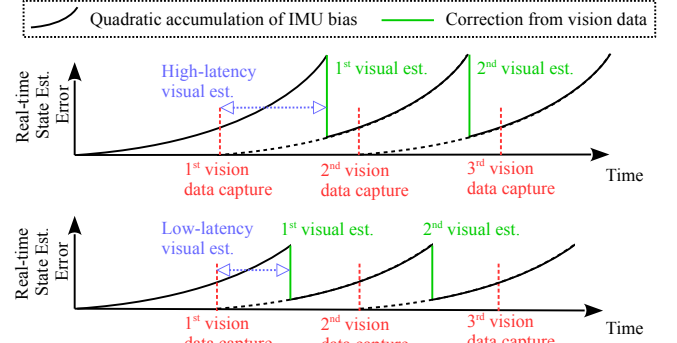


Fig. 1. Impact of visual processing latency in VI-SLAM (best viewed in color). Assuming 100% correct visual estimation and purely-random IMU noise, the only source of error in visual-inertial state estimation is accumulated IMU bias (quadratic in time). **Top:** trend of visual-inertial state estimation error when visual estimation takes 75% of the visual processing budget. **Bottom:** same error trend when visual estimation takes 50% of the budget. Reduced latency yields a reduced state estimation error.

open-loop evaluation fails to fully address the coupled impact of navigation and VI-SLAM estimation during closed-loop operation. For targeted closed-loop navigation, it is hard to gain insights on VI-SLAM from published open-loop benchmark scores. To address this benchmarking gap, we present an open-source [1], reproducible benchmarking simulation for closed-loop VI-SLAM evaluation, and the outcomes from evaluating several VI-SLAM methods using it. Reproducible, closed-loop benchmarking should serve to guide future VI-SLAM research for mobile robotics.

Though VI-SLAM drift is a critical factor influencing closed-loop navigation performance, the latency of visual estimation may also play an important role when in closed-loop. As illustrated in Fig. 1, latency-reduction on the visual processing sub-system could improve the accuracy of fused visual-inertial state estimate due to the quadratic (in time) nature of accumulated IMU bias. Therefore, this paper studies the impact of both drift and visual estimation latency of VI-SLAM with closed-loop benchmarking simulation, by implementing and testing several published VI-SLAM systems with different run-time properties. The closed-loop benchmarking outcomes suggest that VI-SLAM systems must balance drift and latency.

II. RELATED WORKS

This section first reviews existing works on visual-inertial state estimation for closed-loop navigation. The term **VI-SLAM** will be used to indicate both visual-inertial odometry (VIO) and visual-inertial SLAM. After, it reviews evaluation methods for VI-SLAM with a discussion of benchmarking for closed-loop trajectory tracking.

¹Y. Zhao, J.S. Smith, S.H. Karumanchi, and P.A. Vela are with the School of Electrical and Computer Engineering, Georgia Institute of Technology, Atlanta, Georgia, USA. {yipu.zhao, jssmith, skarumanchi3, pvela}@gatech.edu. This work was supported by the National Science Foundation (Award #1816138).

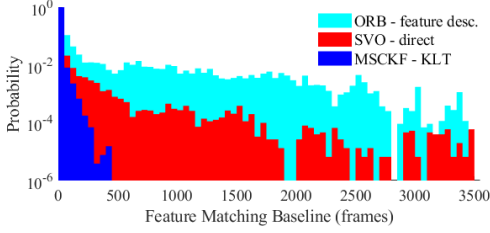


Fig. 2. Distributions of feature matching baselines for 3 commonly used image processing front-ends as computed for the EuRoC MAV benchmark [21]: feature descriptors in ORB-SLAM (ORB) [22], KLT in MSCKF [7], and direct SVO [17]. For each feature/patch, the baseline is assessed by the *length of life*: from the first-measured frame to the last-measured frame. The feature-based front-end (ORB) extracts more long-baseline feature matchings than the KLT and direct methods.

A. VI-SLAM in Closed-Loop Navigation

There is a long history of using filters in visual-inertial state estimation for mobile robots (e.g., EKF [2]; MSCKF [3]; [4]). The combination of sparse optical flow (e.g., KLT [5]) and MSCKF has been recognized as an efficient VI-SLAM solution [6]–[8]. A downside of most filter-based methods is the low mapping quality, which affects long-term navigation with location revisits.

VI-SLAM running Bundle Adjustment (BA) retains an explicit map, which promotes higher accuracy and long-term robustness of state estimation. To bound the cubic computational cost of BA, BA-based VI-SLAM typically works with a subset of historical information (keyframes and landmarks) sub-selected using a sliding window [9] or a covisibility graph [10]. Representative BA-based VI-SLAM includes feature-based OKVIS [11], KLT-based VINS-Fusion [12] and Kimera [13]. Closed-loop navigation with OKVIS has been demonstrated on both ground [14] and aerial robots [15]. Full navigation has been demonstrated with VINS-Fusion on a micro-air vehicle (MAV) [16]. Kimera [13] estimates 3D mesh on-the-fly, which benefits navigation.

Recently direct VI-SLAM systems have been derived; they do not require explicit feature extraction and matching. Direct systems jointly solve data association and state estimation by optimizing an objective functional using raw image readings. Direct VI-SLAM systems such as SVO [17] and ROVIO [18] have been integrated into closed-loop navigation systems [19], [20]. While both KLT and direct VI-SLAM are computationally cheaper than feature-based VI-SLAM, they are more sensitive to navigation-based conditions: e.g. they require accurate pose prediction (from inertial) and minimal light condition changes. Furthermore, both KLT and direct methods are mostly characterized by short-baseline feature matches. Feature descriptor matching, on the other hand, can find reliable long-baseline feature matches for improved state estimation (see Fig. 2).

B. Evaluation of Closed-Loop Trajectory Tracking

Open-loop evaluation of different VI-SLAM methods has been extensively conducted in the literature, e.g. on multiple datasets [23], [24], on multiple computation devices [25]–[27], and for multiple synthetic environments [28], [29]. Closed-loop evaluation of different VI-SLAM methods in

navigation tasks, however, is investigated less. On-board evaluation tends to be reported for individual implementations [4], [30]. One challenge of closed-loop evaluation is that closed-loop navigation is not just a software problem; the performance of the full system is affected by sensor choice, computational resources, system dynamics, and target environment. All these factors need to be experimentally controlled to comprehensively evaluate the performance of closed-loop navigation using VI-SLAM.

One way to conduct comprehensive and repeatable closed-loop evaluation is via simulation. Several existing simulators are commonly used in the robotics community. Gazebo [31] is one of the most popular simulators, with MAV-specific extensions such as RotorS [32]. AirSim [33] is another choice, with photorealistic renderings of visual data via Unreal Engine. A more recent development incorporates hardware in the loop [34]. The approach captures the trajectory of the actual robot on the fly, while rendering virtual visual data on a remote workstation to collect actual data under real physics and virtual data from an easy-to-extend renderer. However, ground truth acquisition relies on a MoCap device, which is hard to scale beyond room-sized environment. To properly benchmarking VI-SLAM in closed-loop navigation, the benchmarking framework needs to be re-configurable to cover a variety of factors, such as sensor configurations, computational & robot platforms, and target environments. Furthermore, ground truth coverage is required over the entire course of navigation. This work aims to fill a existing gap by presenting an open-source, closed-loop benchmarking framework that supports the above requirements, and serves to provide performance insights on representative VI-SLAM systems based on the closed-loop evaluation results.

III. CLOSED-LOOP SYSTEM OVERVIEW

The closed-loop trajectory tracking system consists of two major subsystems, illustrated in Fig. 3 and described as: 1) a VI-SLAM system taking vision & inertial data to generate high-rate state estimates and low-rate map updates; and 2) a controller using high-rate output from the pose tracking module of VI-SLAM to generate actuator commands. Though this paper covers only stereo-inertial sensory inputs, the system supports other common visual sensors such as monocular and RGB-D cameras.

While both mapping and loop closing are essential for accurate and robust state estimation, these two modules require high computation, and typically operate at a much lower rate than pose tracking (usually by an order of magnitude). Therefore the high-rate pose estimation required in feedback control is collected by the pose tracking module. This study explores the efficiency and accuracy of the pose tracking module when used for feedback. A variety of VI-SLAM systems are integrated into the closed-loop system, covering representative design options such as loosely/tightly-coupled visual-inertial fusion, direct/feature-based data association, and filter/BA-based back-end.

The focus of this study is the trajectory tracking performance of VI-SLAM systems when used in the closed-loop.

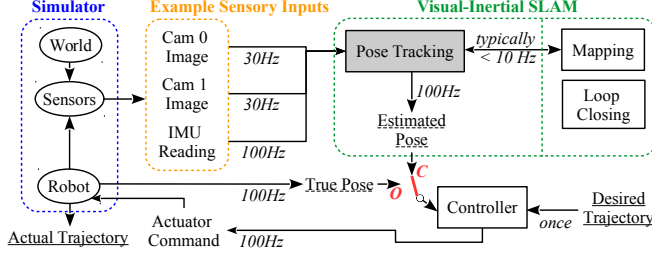


Fig. 3. Overview of the closed-loop trajectory tracking system. The Gazebo simulator sends out sensory data to VI-SLAM. The pose-tracking module of VI-SLAM processes the data, and outputs high-rate pose estimation. In closed-loop benchmarking (red switch at “C”), the pose estimation is taken by the controller to generate high-rate actuator command, which is sent back to the simulated robot in Gazebo. Performance is quantified by comparing desired and actual trajectories (solid underlined text). In open-loop benchmarking (red switch at “O”), the controller generates commands based on the true pose, available from the simulator. Performance is quantified by comparing true and estimated poses (dashed underlined text).

The tracking performance can be reflected by computing the pose error between the desired and actual trajectories, accumulated over the entire course of navigation. Here we report the root mean square of the translation error between the desired and actual trajectories, dubbed tracking RMSE, as the performance metric. Tracking RMSE matches the formulation of ATE [35], commonly used in open-loop evaluation, but works with actual robot trajectory. It directly measures the end performance of the trajectory tracking system, thereby capturing the joint effect of pose tracking drift and latency. Additional metrics that capture orientation error are reported online (see [1]).

The mobile robot used in the simulation is the differential drive TurtleBot2. Mounted to the robot are a 30fps stereo camera with an 11cm baseline, and an IMU placed at its base. Data streams from both the stereo camera and IMU are input to the VI-SLAM system, which outputs $SE(3)$ state estimates. The trajectory tracking controller uses the $SE(2)$ subspace of the $SE(3)$ estimate to track the target trajectory. The next subsections describe the implemented VI-SLAM systems, the trajectory tracking controller, and the simulation setup in Gazebo/ROS.

A. Visual-Inertial SLAM Systems

Several publicly available stereo(-inertial) SLAM implementations were selected for integration into the closed-loop benchmarking system. The five implementations are:

- 1) *MSC*: MSCKF-VIO [7] + MSF [36]. MSCKF-VIO is a tightly-coupled VIO system, with KLT-based front-end and MSCKF back-end. EKF-based sensor fusion, MSF [36], densifies the low-rate estimation output from MSCKF-VIO, before sending it to controller. No loop closing is included.
- 2) *VINS*: VINS-Fusion [12] is a tightly-coupled VI-SLAM with KLT-based front-end and BA-based back-end. *VINS* has a large latency due to the BA. It does provide a low-latency, high-rate IMU propagation signal, which is sent to controller. *VINS* comes with loop closing, which is preferred in long-term revisit scenarios. A circular motion is executed to initialize *VINS* prior to starting the SLAM

estimation process.

- 3) *SVO*: SVO [17] + MSF. An efficient, loosely-coupled VIO system that consists of direct SVO and MSF fusion. No loop closing module. *SVO* has the lowest pose tracking latency of the methods listed.
- 4) *ORB*: ORB-SLAM [22] + MSF. ORB-SLAM has a feature-based front-end and BA-based back-end. Due to the computational-costly feature extraction and matching, ORB-SLAM has a large visual estimation latency. Similar with *MSC* and *SVO*, MSF is integrated into ORB to generate a high-rate estimation signal.
- 5) *GF*: Lazy-GF-ORB-SLAM [24] + MSF. A loosely-coupled modified version of *ORB* with two efficiency modifications: good feature and lazy stereo. Good feature matching performs targeted map-to-frame matching under an upper bounded matching budget. The lazy stereo modification partitions the stereo ORB-SLAM computations into those necessary for immediate pose estimation versus those that assist future pose estimation computations. The former is prioritized to run first, therefore enabling more rapidly output of pose estimation. These two modifications lower the latency without significant impact on the accuracy of pose estimation.

If no initialization approach is described, then the default is to keep the robot static for 10 seconds before starting a closed-loop/open-loop run.

B. Feedback Control

The desired trajectory $d^*(t) \in \mathbb{R}^2$ is constructed from a series of specified waypoints using splines. An exponentially stabilizing trajectory tracking controller for Hilare-style robots [37] generates a kinematically feasible trajectory for the robot to follow. In the following discussion, constraints on accelerations and velocities are omitted for clarity, though they exist within the actual implementation.

The robot pose as a function of time $g(t) \in SE(2)$ obeys follows the control equations:

$$\dot{g} = g \cdot \begin{bmatrix} \nu \\ 0 \\ \omega \end{bmatrix} \quad \text{and} \quad \begin{matrix} \dot{\nu} = u^1 \\ \dot{\omega} = u^2 \end{matrix} \quad (1)$$

where ν is the forward velocity and ω is the angular velocity, both in the body frame. The signal $u = (u^1, u^2)^T$ coordinates are the forward and angular acceleration (in body frame).

The controller used relies on the differential flatness of the robot motion to achieve exponential stabilization of a virtual point in front of the robot (by a distance λ) [37]. Define the λ -adjusted rotation matrix and angular velocity matrix,

$$R_\lambda = R \cdot \text{diag}(1, \lambda) \quad \text{and} \quad \hat{\omega}(\lambda, \dot{\lambda}) = \begin{bmatrix} 0 & -\lambda\omega \\ \frac{1}{\lambda}\omega & \dot{\lambda} \end{bmatrix}, \quad (2)$$

where R is the rotation matrix given by the orientation in g . For e_1 the unit body \hat{x} -vector in the world frame, the trajectory tracking control law is

$$u = c_p R_\lambda^{-1} (d^* - d - \lambda * R e_1) + c_d \left(R_\lambda^{-1} \dot{d}^* - V \right) - c_d \dot{\lambda} e_1 - \hat{\omega}(\lambda, \dot{\lambda}) V - (\hat{\omega}(\lambda, \dot{\lambda}) - c_\lambda I) \dot{\lambda} e_1, \quad (3)$$

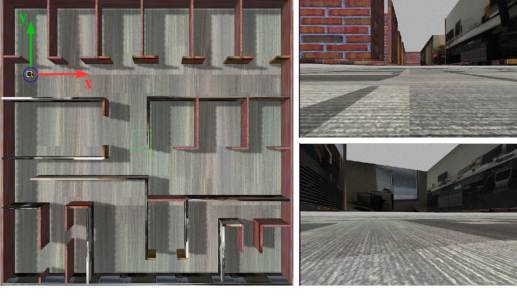


Fig. 4. The virtual office world. **Left:** Top-down view. The robot starts at the top-left corner, facing the long corridor. **Right:** Example images captured by on-board stereo camera (left camera).

where c_p, c_d, c_λ are feedback gains and $V = [\nu | \omega]^T$. The additional offset dynamics are

$$\dot{\lambda} = -c_\lambda(\lambda - \epsilon), \text{ where } \lambda(0) > \epsilon > 0, c_\lambda > 0. \quad (4)$$

The dynamical system represented by Eqs 1-4 yields a reference trajectory of robot poses $g^*(t)$ and body velocity components $V^*(t)$ for tracking the desired trajectory $d^*(t)$. The offset variable $\lambda^*(t)$ can be ignored.

The real time trajectory controller drives the robot to track the reference trajectory based on feedback of the robot's estimated state (an $SE(2)$ substate of the $SE(3)$ state estimate). These control commands are:

$$\begin{aligned} \nu_{cmd} &= k_x * \tilde{x} + \nu^* \\ w_{cmd} &= k_\theta * \tilde{\theta} + k_y * \tilde{y} + \omega^* \end{aligned} \quad (5)$$

where $[\tilde{x}, \tilde{y}, \tilde{\theta}]^T \simeq \tilde{g} = g^{-1}g^*$ is the relative pose error between the current state g and the desired state g^* in body frame. In the absence of error, the control signal is $V^*(t)$.

C. Simulation Setup

This section describes the Gazebo-simulated environment for testing closed-loop trajectory tracking with VI-SLAM systems. The scene created for robot navigation is a virtual office world (Fig. 4). The world is based on the floor-plan of an actual office, with texture-mapped surfaces. The walls are placed 1m above the ground plane since collision checking and path planning is outside the scope of this paper. Introducing collision avoidance would add another coupling factor to the closed-loop system, which would introduce unneeded difficulty in identifying the source of tracking error (i.e., was it to avoid a collision or due to poor estimation?).

Six test trajectories were created for the closed-loop navigation experiments, each with different characteristics (Fig. 5). The first two are relatively short (~ 50 m), with few to no revisits. The 3rd and 4th trajectories are both of medium length (~ 120 m). The 3rd has many revisits as it retraces the trajectory once, whereas the 4th crosses earlier trajectory segments facing the opposite direction or transverse to them. The last 2 trajectories are long (~ 240 m). The 5th retraces trajectory segments, while the 6th does so facing in the opposite direction. All trajectories have the same start point for the robot, the origin of the world. Three desired linear velocities are tested: 0.5m/s, 1.0m/s, and 1.5m/s. Based on these velocities, the navigation course in simulation lasted from 30 seconds up to 480 seconds.

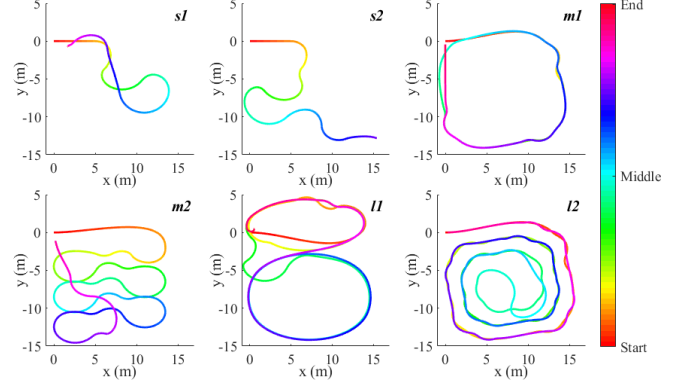


Fig. 5. All 6 desired trajectories used in closed-loop navigation experiments. Each desired trajectory is color-coded to show the direction of travel.

IV. EXPERIMENTAL RESULTS

This section describes the outcomes of two main experiments. The first involves open-loop evaluation of the stereo VI-SLAM methods, where the controller takes true poses instead of VI-SLAM estimations (red "O" in Fig. 3). The open-loop evaluation serves two purposes: 1) it demonstrates that the relative ranking of the methods in the simulated world is roughly preserved when compared to video-recorded open-loop benchmarks such as EuRoC [21], and 2) it characterizes the functional domain of the simulation environment relative to the benchmarks. The second experiment performs closed-loop trajectory tracking tests, where the controller is fed with VI-SLAM estimation (red "C" in Fig. 3). The objective of closed-loop benchmarking is to identify the VI-SLAM properties (i.e., drift, latency) that have impact on trajectory tracking performance.

All 5 VI-SLAM systems parameter configurations were found via parameter sweep. For each test configuration (desired trajectory, desired linear velocity, VI-SLAM method, and IMU), the benchmarking run is repeated five times, so that random factors such as multi-threading and random sensory noise are properly reflected. Two commonly-used IMUs are simulated: a high-end ADIS16448 and a low-end MPU6000. Open-loop benchmarking was performed on an i7-4770 (single thread Passmark score: 2228). Closed-loop benchmarking was performed on a dual Intel Xeon E5-2680 workstation (single thread Passmark score: 1661). For reference, most published closed-loop navigation systems [4], [7], [8], [15], [16], [20], [38] employ an Intel NUC whose CPUs score between 1900-2300 (single thread). The full stack, including the simulator, integrated VI-SLAM systems and trajectory tracking controller, are released [1].

A. Open-Loop Outcomes and Analysis

Given that simulation and recorded open-loop benchmark data may not align, this section conducts a comparison for verification of the domain of applicability for the simulation. The comparison shows that simulated scenes have some overlap with existing benchmarks though they do not span the entire domain. Based on the similarity, closed-loop implementations should have predictive power when the closed-loop system is deployed in equivalent real-world settings.

TABLE I
CHARACTERIZATION OF BENCHMARKS

Seq.	Duration	Motion	Revisit	Feats.
<i>MH 03 med</i>	medium	medium	high	235
<i>MH 04 diff</i>	short	high	high	235
<i>VR1 01 easy</i>	medium	medium	high	227
<i>VR2 02 med</i>	short	medium	high	246
<i>MH 05 diff</i>	short	high	high	240
<i>s1</i>	short	low-high	low	131
<i>s2</i>	short	low-high	low	126
<i>m1</i>	short	low-high	high	122
<i>m2</i>	medium	low-high	low	115
<i>l1</i>	medium	low-high	high	121
<i>l2</i>	medium	low-high	med	114

A subset of the EuRoC sequences and the simulated open-loop sequences are characterized in Table I, using the benchmark properties evaluated in [39]. The duration profile is defined with medium describing an interval of [2, 10] minutes. The motion profile is categorized from *low* (0.5 m/s) to *medium* (1.0 m/s) to *high* (1.5 m/s). The revisit frequency is a function of the trajectory followed and how often there is co-visibility of features across trajectory segments that are temporally distant. One additional statistic captured is the average number of features tracked per frame using *ORB* (last column). Simulation sequences exhibit less texture than EuRoC ones. There is sufficient overlap in the characteristics of the two benchmarks, with the simulation reflecting slightly more diverse scenarios. Qualitatively, the simulation sequences are comparable or harder benchmarking cases relative to the EuRoC sequences.

To compare further, we ran open-loop benchmarking against ground truth to get a sense for the pose estimation properties of the VI-SLAM algorithms and whether the two benchmark sets agree in terms of relative ordering. The results averaged from 5-run repeats of the *medium* motion profile are summarized in Tables II and III, where the track loss cases are omitted (dashes). According to the tables, the ATE between VI-SLAM estimation and ground truth is usually lower for EuRoC sequences. Both *SVO* and *VINS* exhibit outliers in EuRoC relative to the prevailing values across all methods, with *SVO* having one and *VINS* having three. They occur for the *MH* sequences, suggesting that these might be more problematic in general for *VINS* and *SVO*. However, *SVO* and *VINS* also have one track failure for the simulated cases. Overall, the outcomes align with the previous claim that the simulation sequences are comparable to or harder than EuRoC. If track failure is added as a penalty to the simulation performance outcomes, then the rank ordering of the algorithms agree between EuRoC and simulation. *GF* typically has the lowest ATE, while *VINS* has the highest ATE. Furthermore, the relative orders of latencies for different VI-SLAM agree: *SVO* is lowest, and *VINS* is highest (*MSC* is unique in that it has mismatch). The comparisons support using simulation to benchmark VI-SLAM, with validity for specific deployment conditions.

B. Closed-Loop Outcomes and Analysis

Trajectory tracking performance is quantified in Tables IV and V. The tracking RMSE between the desired and actual

trajectories reflects an average of the 5-run repeats. Cases with average RMSE over 10m are considered navigation failures and omitted (dashes). The average latency of visual estimation in each VI-SLAM is reported in the bottom row of each table (algorithms sorted to be in ascending order).

According to Tables IV and V, both *VINS* and *ORB* fail under multiple configurations. Compared to *ORB*, the success rate and RMS of *GF* are significantly improved. The reduction of visual estimation latency contributes to the improvement, since the open-loop outcomes of *ORB* and *GF* are similar in terms of drift, but are quite different in terms of latency. The outcomes suggest that meeting standard frame-rate latency levels (~ 30 ms) is best, and quite possibly essential for good closed-loop trajectory tracking performance. The filter-based *MSC* is significantly affected by the IMU data quality, as it fails to navigate for multiple low-end IMU cases and higher velocity. The outcomes suggest an over-reliance on the IMU for pose estimation, which is supported by Fig. 2 where *MSC* has poor long-term data association for detected features. Being able to re-associate to lost tracks improves performance by linking against a known static point in the world and improving absolute position estimates. Otherwise, systems such as *MSC* rely on integrated estimates which have poor observability properties.

The last two approaches to review are *SVO* and *GF*, which both successfully track the camera pose for all but one sequence, each. These are the two strongest performing methods. Interestingly they have different run-time properties. For both the open-loop and closed-loop evaluations, *SVO* has the lowest latency but the highest drift, while *GF* is the opposite. Their relative performance remained the same from open-loop to closed-loop, modulo a small fraction of sequences. It appears that low latencies are tolerant to higher drift, whereas lower drift permits higher latency. Overall, however, it appears that once the latency is low enough, it is better to target accuracy enhancements over latency enhancements for closed-loop trajectory tracking (for ground vehicles in mostly static, feature sufficient, environments). Comparing *SVO* and *GF* across the two IMU types indicates that high-end IMUs provide the best error scaling to ground speed, with *GF* being more consistent as the speed increased.

These quantitative outcomes can be seen qualitatively in Fig. 6 and 7, which trace the closed-loop robot trajectories for the different VI-SLAM methods. *VINS* goes out of bounds for many runs. Focusing on the traces of *SVO* and *GF*, it is clear that *SVO* has a higher estimation variance across the runs for a given sequence, while *GF* trajectories are more closely clustered. The properties hold irrespective of the IMU type. Overall, *GF* appears to be the strongest performer. As a modification of *ORB*, it seeks to reduce pose estimation latency while preserving the beneficial properties of *ORB*. The findings of this paper imply that prioritizing accuracy while striving to achieve sufficiently small latencies is an effective means to identifying a high performing VI-SLAM for autonomous, mobile robot applications. Some work is still needed to resolve the outlier cases for *GF*.

TABLE II

OPEN-LOOP OUTCOMES ON EUrOC (ATE IN M; LATENCY IN MS)

Seq.	SVO	MSC	GF	ORB	VINS
<i>MH 03 med</i>	0.31	0.24	0.07	0.05	1.50
<i>MH 04 diff</i>	2.78	0.28	0.10	0.15	2.24
<i>VR1 01 easy</i>	0.05	0.12	0.10	0.04	0.35
<i>VR2 02 med</i>	0.19	0.22	0.04	0.09	0.35
<i>MH 05 diff</i>	0.47	0.28	0.04	0.20	2.32
Avg. ATE	0.76	0.23	0.07	0.11	1.35
Avg. Latency	16.4	28.3	20.7	38.5	93.5

TABLE III

OPEN-LOOP SIMULATION OUTCOMES (ATE IN M; LATENCY IN MS)

Seq.	SVO	MSC	GF	ORB	VINS
<i>s1</i>	0.15	0.21	0.12	0.14	0.14
<i>s2</i>	0.12	0.14	0.11	0.38	0.13
<i>m1</i>	0.33	0.32	0.19	0.16	–
<i>m2</i>	0.45	0.29	0.19	0.20	0.33
<i>l1</i>	0.42	0.57	0.25	0.09	0.57
<i>l2</i>	–	0.51	0.29	0.38	0.47
Avg. ATE	0.29	0.34	0.19	0.23	0.32
Avg. Latency	9.3	14.2	26.2	47.5	62.0

TABLE IV

CLOSED-LOOP OUTCOMES WITH HIGH-END IMU ADIS16448 (TRACKING RMSE IN M; LATENCY IN MS)

Seq.	0.5m/s					1.0m/s					1.5m/s				
	SVO	MSC	GF	ORB	VINS	SVO	MSC	GF	ORB	VINS	SVO	MSC	GF	ORB	VINS
<i>s1</i>	0.23	0.65	0.11	0.24	–	0.56	0.26	0.12	0.28	1.36	0.49	0.22	0.14	0.23	0.37
<i>s2</i>	0.18	0.46	0.09	0.43	–	1.13	0.38	0.08	–	–	1.21	0.33	0.09	3.26	–
<i>m1</i>	0.92	1.54	0.12	0.31	–	–	1.01	0.10	0.23	–	1.26	0.81	0.11	2.10	–
<i>m2</i>	0.36	2.23	0.14	–	–	0.86	1.53	0.12	–	–	1.87	0.68	0.14	–	–
<i>l1</i>	2.12	2.73	–	–	–	1.79	6.67	0.15	–	–	1.22	2.13	0.22	–	–
<i>l2</i>	0.87	2.62	0.36	0.24	–	1.27	3.25	0.35	0.31	–	2.78	2.66	0.35	0.37	–
Avg. RMS	0.78	1.70	0.16	0.30	–	1.12	2.18	0.15	0.27	1.36	1.47	1.14	0.18	1.49	0.37
Avg. Latency	8.9	17.7	32.8	52.4	55.0	8.9	16.9	32.4	51.7	73.9	8.9	16.7	32.0	50.6	64.1

TABLE V

CLOSED-LOOP OUTCOMES WITH LOW-END IMU MPU6000 (TRACKING RMSE IN M; LATENCY IN MS)

Seq.	0.5m/s					1.0m/s					1.5m/s				
	SVO	MSC	GF	ORB	VINS	SVO	MSC	GF	ORB	VINS	SVO	MSC	GF	ORB	VINS
<i>s1</i>	0.68	0.29	0.13	0.05	0.52	1.21	0.35	0.16	0.25	0.89	2.30	–	0.41	0.46	–
<i>s2</i>	0.62	0.40	5.00	0.96	–	0.96	0.35	0.10	–	–	2.68	–	0.21	–	–
<i>m1</i>	1.53	0.68	0.26	0.19	8.24	3.21	–	0.28	1.21	–	3.95	–	0.36	–	–
<i>m2</i>	2.13	1.60	0.43	–	–	2.33	–	0.53	–	–	4.21	–	0.39	–	–
<i>l1</i>	0.18	4.60	3.24	1.62	–	2.19	–	0.37	–	–	2.46	1.87	3.41	–	–
<i>l2</i>	0.21	3.74	0.36	–	–	2.46	5.67	0.35	–	–	1.86	1.92	0.32	–	–
Avg. RMS	0.89	1.88	1.57	0.71	4.38	2.06	2.12	0.30	0.73	0.89	2.91	1.90	0.85	0.46	–
Avg. Latency	10.1	17.4	28.9	53.2	62.3	10.0	16.9	31.5	53.0	65.4	10.0	16.5	31.8	52.8	58.8

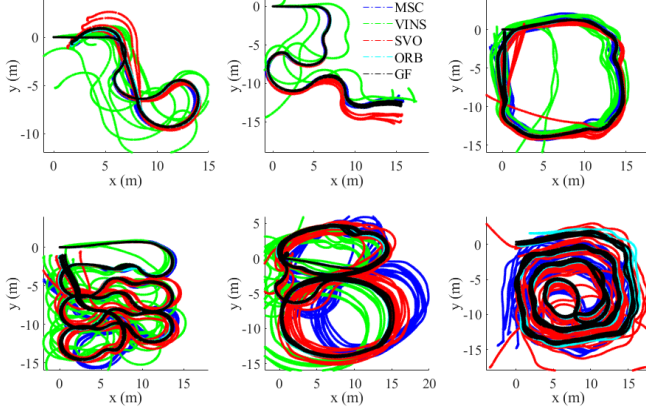


Fig. 6. Actual trajectories the robot traveled for each desired trajectory, color-coded by method. Desired velocity is 1.0m/s and IMU is high-end.

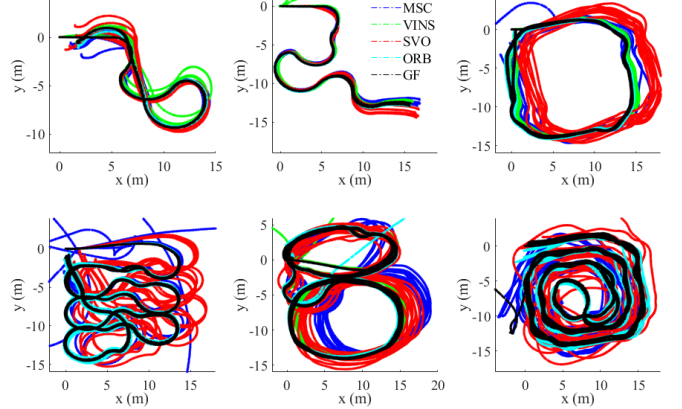


Fig. 7. Actual trajectories the robot traveled for each desired trajectory, color-coded by method. Desired velocity is 1.0m/s and IMU is low-end.

V. CONCLUSION

This paper investigated several stereo VI-SLAM methods to understand their closed-loop trajectory tracking properties. The study was supported with a simulated Gazebo environment shown to be representative of a specific set of benchmark conditions. Analysis of the outcomes showed that both latency and drift play important roles in achieving accurate trajectory tracking. A VI-SLAM system built upon ORB-SLAM, denoted by *GF*, provides the most accurate

trajectory tracking outcomes, which is consistent with its open-loop performance. Other methods were less consistent; SVO has high performance in closed-loop but poor performance in open-loop, and ORB vice-versa. Future work will extend the benchmarking environments with additional mobile robots, rendering options, and visual environments or settings. Importantly, integration with actual collision-avoidance systems and the impact of environmental obstacles on SLAM will improve the task-realism of the benchmark.

REFERENCES

- [1] Y. Zhao, J. Smith, S. Karumanchi, and P. Vela, "ClosedLoopBench: Meta package for IVALab's closed-loop SLAM benchmarking in Gazebo/ROS," <https://github.com/ivalab/meta-ClosedLoopBench>, 2020.
- [2] A. Howard, "Real-time stereo visual odometry for autonomous ground vehicles," in *IEEE/RSJ International Conference on Intelligent Robots and Systems*, 2008, pp. 3946–3952.
- [3] A. I. Mourikis and S. I. Roumeliotis, "A multi-state constraint Kalman filter for vision-aided inertial navigation," in *IEEE International Conference on Robotics and Automation*, 2007, pp. 3565–3572.
- [4] I. Cvišić, J. Česić, I. Marković, and I. Petrović, "Soft-SLAM: Computationally efficient stereo visual simultaneous localization and mapping for autonomous unmanned aerial vehicles," *Journal of Field Robotics*, vol. 35, no. 4, pp. 578–595, 2018.
- [5] J. Shi and C. Tomasi, "Good features to track," in *IEEE Conference on Computer Vision and Pattern Recognition*, 1994, pp. 593–600.
- [6] G. Loianno, C. Brunner, G. McGrath, and V. Kumar, "Estimation, control, and planning for aggressive flight with a small quadrotor with a single camera and IMU," *IEEE Robotics and Automation Letters*, vol. 2, no. 2, pp. 404–411, 2017.
- [7] K. Sun, K. Mohta, B. Pfommer, M. Watterson, S. Liu, Y. Mulgaonkar, C. J. Taylor, and V. Kumar, "Robust stereo visual inertial odometry for fast autonomous flight," *IEEE Robotics and Automation Letters*, vol. 3, no. 2, pp. 965–972, 2018.
- [8] S. Paschall and J. Rose, "Fast, lightweight autonomy through an unknown cluttered environment," in *IEEE Aerospace Conference*, 2017, pp. 1–8.
- [9] G. Sibley, L. Matthies, and G. Sukhatme, "Sliding window filter with application to planetary landing," *Journal of Field Robotics*, vol. 27, no. 5, pp. 587–608, 2010.
- [10] H. Strasdat, A. J. Davison, J. M. Montiel, and K. Konolige, "Double window optimisation for constant time visual SLAM," in *IEEE International Conference on Computer Vision*, 2011, pp. 2352–2359.
- [11] S. Leutenegger, S. Lynen, M. Bosse, R. Siegwart, and P. Furgale, "Keyframe-based visual-inertial odometry using nonlinear optimization," *The International Journal of Robotics Research*, vol. 34, no. 3, pp. 314–334, 2015.
- [12] T. Qin, J. Pan, S. Cao, and S. Shen, "A general optimization-based framework for local odometry estimation with multiple sensors," *arXiv preprint arXiv:1901.03638*, 2019.
- [13] A. Rosinol, M. Abate, Y. Chang, and L. Carlone, "Kimera: an open-source library for real-time metric-semantic localization and mapping," in *IEEE International Conference on Robotics and Automation*, 2020.
- [14] F. Blochliger, M. Fehr, M. Dymczyk, T. Schneider, and R. Siegwart, "Topomap: Topological mapping and navigation based on visual SLAM maps," in *IEEE International Conference on Robotics and Automation*, 2018, pp. 1–9.
- [15] M. Burri, H. Oleynikova, M. W. Achtelik, and R. Siegwart, "Real-time visual-inertial mapping, re-localization and planning onboard MAVs in unknown environments," in *IEEE/RSJ International Conference on Intelligent Robots and Systems*, 2015, pp. 1872–1878.
- [16] Y. Lin, F. Gao, T. Qin, W. Gao, T. Liu, W. Wu, Z. Yang, and S. Shen, "Autonomous aerial navigation using monocular visual-inertial fusion," *Journal of Field Robotics*, vol. 35, no. 1, pp. 23–51, 2018.
- [17] C. Forster, Z. Zhang, M. Gassner, M. Werlberger, and D. Scaramuzza, "SVO: Semidirect visual odometry for monocular and multicamera systems," *IEEE Transactions on Robotics*, vol. 33, no. 2, pp. 249–265, 2017.
- [18] M. Bloesch, M. Burri, S. Omari, M. Hutter, and R. Siegwart, "Iterated extended Kalman filter based visual-inertial odometry using direct photometric feedback," *The International Journal of Robotics Research*, vol. 36, no. 10, pp. 1053–1072, 2017.
- [19] C. Papachristos, S. Khatkhat, and K. Alexis, "Autonomous exploration of visually-degraded environments using aerial robots," in *IEEE International Conference on Unmanned Aircraft Systems*, 2017, pp. 775–780.
- [20] H. Oleynikova, Z. Taylor, A. Millane, R. Siegwart, and J. Nieto, "A complete system for vision-based micro-aerial vehicle mapping, planning, and flight in cluttered environments," *arXiv preprint arXiv:1812.03892*, 2018.
- [21] M. Burri, J. Nikolic, P. Gohl, T. Schneider, J. Rehder, S. Omari, M. W. Achtelik, and R. Siegwart, "The EuRoC micro aerial vehicle datasets," *The International Journal of Robotics Research*, vol. 35, no. 10, pp. 1157–1163, 2016.
- [22] R. Mur-Artal, J. M. M. Montiel, and J. D. Tardos, "ORB-SLAM: a versatile and accurate monocular SLAM system," *IEEE Transactions on Robotics*, vol. 31, no. 5, pp. 1147–1163, 2015.
- [23] B. Bodin, H. Wagstaff, S. Saeedi, L. Nardi, E. Vespa, J. Mawer, A. Nisbet, M. Luján, S. Furber, A. J. Davison *et al.*, "SLAMBench2: Multi-objective head-to-head benchmarking for visual SLAM," in *IEEE International Conference on Robotics and Automation*, 2018, pp. 1–8.
- [24] Y. Zhao and P. A. Vela, "Good feature matching: Towards accurate, robust VO/VSLAM with low latency," *IEEE Transactions on Robotics*, 2020.
- [25] M. Bujanca, P. Gafton, S. Saeedi, A. Nisbet, B. Bodin, M. O'Boyle, A. Davison, P. Kelly, G. Riley, B. Lennox, M. Lujan, and S. Furber, "SLAMBench 3.0: systematic automated reproducible evaluation of SLAM systems for robot vision challenges and scene understanding," in *ICRA Workshop on Dataset Generation and Benchmarking of SLAM Algorithms for Robotics and VR/AR*, 2019.
- [26] J. Delmerico and D. Scaramuzza, "A benchmark comparison of monocular visual-inertial odometry algorithms for flying robots," *IEEE International Conference on Robotics and Automation*, vol. 10, p. 20, 2018.
- [27] S. Saeedi, B. Bodin, H. Wagstaff, A. Nisbet, L. Nardi, J. Mawer, N. Melot, O. Palomar, E. Vespa, T. Spink *et al.*, "Navigating the landscape for real-time localization and mapping for robotics and virtual and augmented reality," *Proceedings of the IEEE*, no. 99, pp. 1–20, 2018.
- [28] A. Antonini, W. Guerra, V. Murali, T. Sayre-McCord, and S. Karaman, "The blackbird dataset: A large-scale dataset for UAV perception in aggressive flight," in *International Symposium on Experimental Robotics*, 2018.
- [29] W. Li, S. Saeedi, J. McCormac, R. Clark, D. Tzoumanikas, Q. Ye, Y. Huang, R. Tang, and S. Leutenegger, "InteriorNet: Mega-scale multi-sensor photo-realistic indoor scenes dataset," in *British Machine Vision Conference*, 2018.
- [30] A. Weinstein, A. Cho, G. Loianno, and V. Kumar, "Visual inertial odometry swarm: An autonomous swarm of vision-based quadrotors," *IEEE Robotics and Automation Letters*, vol. 3, no. 3, pp. 1801–1807, 2018.
- [31] N. Koenig and A. Howard, "Design and use paradigms for Gazebo, an open-source multi-robot simulator," in *IEEE/RSJ International Conference on Intelligent Robots and Systems*, vol. 3, 2004, pp. 2149–2154.
- [32] F. Furrer, M. Burri, M. Achtelik, and R. Siegwart, "RotorS: A modular Gazebo MAV simulator framework," in *Robot Operating System*. Springer, 2016, pp. 595–625.
- [33] S. Shah, D. Dey, C. Lovett, and A. Kapoor, "AirSim: High-fidelity visual and physical simulation for autonomous vehicles," in *Field and Service Robotics*. Springer, 2018, pp. 621–635.
- [34] T. Sayre-McCord, W. Guerra, A. Antonini, J. Arneberg, A. Brown, G. Cavalheiro, Y. Fang, A. Gorodetsky, D. McCoy, S. Quilter *et al.*, "Visual-inertial navigation algorithm development using photorealistic camera simulation in the loop," in *IEEE International Conference on Robotics and Automation*, 2018, pp. 2566–2573.
- [35] J. Sturm, W. Burgard, and D. Cremers, "Evaluating egomotion and structure-from-motion approaches using the TUM RGB-D benchmark," in *Workshop on Color-Depth Camera Fusion in Robotics at the IEEE/RJS International Conference on Intelligent Robot Systems*, 2012.
- [36] S. Lynen, M. W. Achtelik, S. Weiss, M. Chli, and R. Siegwart, "A robust and modular multi-sensor fusion approach applied to MAV navigation," in *IEEE/RSJ International Conference on Intelligent Robots and Systems*, 2013, pp. 3923–3929.
- [37] R. Olfati-Saber, "Near-identity diffeomorphisms and exponential epsi-tracking and epsi-stabilization of first-order nonholonomic SE(2) vehicles," in *IEEE American Control Conference*, vol. 6, 2002, pp. 4690–4695.
- [38] D. Scaramuzza, M. C. Achtelik, L. Doitsidis, F. Friedrich, E. Kosmatopoulos, A. Martinelli, M. W. Achtelik, M. Chli, S. Chatzichristofis, L. Kneip *et al.*, "Vision-controlled micro flying robots: from system design to autonomous navigation and mapping in GPS-denied environments," *IEEE Robotics & Automation Magazine*, vol. 21, no. 3, pp. 26–40, 2014.

- [39] W. Ye, Y. Zhao, and P. A. Vela, “Characterizing SLAM benchmarks and methods for the robust perception age,” *Workshop on Dataset Generation and Benchmarking of SLAM Algorithms for Robotics and VR/AR at the IEEE International Conference on Robotics and Automation*, 2019.